High resolution digital image correlation for microstructural strain analysis of a stainless steel repaired by Directed Energy Deposition

Yanis Balit, Camille Guévenoux, Alexandre Tanguy, Manas V Upadhyay, Eric Charkaluk, Andrei Constantinescu

High resolution digital image correlation for microstructural strain analysis of a stainless steel repaired by Directed Energy Deposition

Yanis Balit[a], Camille Guévenoux[a,b], Alexandre Tanguy[a], Manas V. Upadhyay[a], Eric Charkaluk[a], Andrei Constantinescu[a,*]

[a] *Laboratoire de mécanique des solides - CNRS, École Polytechnique, Institut Polytechnique de Paris, 91128 Palaiseau, France*
[b] *Computational Solid Mechanics, Safran, 78114 Magny-les-Hameaux, France*

Abstract

Deformations within a microstructural gradient zone of stainless steel repaired specimens are investigated. The repair, added material by Directed Energy Deposition over a hot rolled sheet substrate, was tested in monotonic tensile experiments. In situ tests, scanning electron microscope images combined with high resolution digital image correlation and electron backscatter diffraction maps, permitted to monitor the local strain distribution. The strain distribution is homogeneous in the substrate and exhibits a heterogeneous pattern in the printed part with localization correlating spatially with the position of interlayers. The vicinity of the interface has smaller strains and exhibits larger hardness.

Keywords:
Directed Energy Deposition, high resolution digital image correlation, electron backscatter diffraction maps, strain map, repair

*Corresponding author: andrei.constantinescu@polytechnique.edu

1. Introduction

Additive manufacturing allows to repair components by the direct addition of material over the damaged zone. In particular, Directed Energy Deposition (DED) [1] is a leader in this field. In DED, the powder/wire feedstock is directly injected into a moving heat-source (laser or electron-beam) which melts the material. After deposition, the molten material undergoes complex melt-pool dynamics and a rapid cooling in the solid state. Addition of further layers subjects the material to heating-cooling thermal cycles at varying temperature rates. These phenomena are driven by process parameters and generate a hierarchical microstructure [2; 3] that is different from conventionally processed materials. It further implies that the original part and the repaired material exhibit very different microstructures. Therefore, under mechanical loading, these differences generate particular load distribution and strain localization, significantly unlike a part with a homogeneous microstructure.

This article proposes an analysis of the gradient of microstructural properties and the associated deformation mechanisms around the jointing interface for repair configurations. For the latter, deformation patterns were obtained through High Resolution Digital Image Correlation (HR-DIC) during an in situ tensile test inside a Scanning Electron Microscope (SEM). The local strain distribution was monitored by associating the HR-DIC data with electron backscatter diffraction (EBSD) maps.

2. Materials and Methods

A single-track thickness wall with the dimension $50 \times 30 \times 0.7\,mm^3$ was deposited by a DED machine on a thin 316L stainless steel (SS316L) hot rolled sheet substrate with the dimension $55 \times 40 \times 0.7\,mm^3$. A back and forth printing strategy was employed with the following DED process parameters: laser power of $225\,W$, deposition speed of $2000\,mm/min$, powder flow of $6.5\,g/min$, pause time between successive deposited layers of $1\,s$ and a vertical spacing between successive layer of $0.12\,mm$. The SS316L powder used had a particle size between $45 - 90\,\mu m$. Further discussions concerning these process parameters are available in [4] .

Three equal dog-bone shaped specimens were extracted by water jet cutting: fully printed (FPS), repaired (RS) and substrate (SS) specimens as presented in Figure 1(a). The RS is composed along the vertical axis of two equal parts: (i) an initial substrate and (ii) the added repaired part. This design permits to load the interface in tension during a tensile experiment.

Ex situ monotonic tensile tests were first performed for the three specimen configurations in order to determine the tensile properties. Then, a RS was prepared with a two-scale gold pattern deposited by lithography on its surface and loaded with a tensile machine inside a scanning electron microscope (SEM) (see [4] for additional details). A "micro grid" ($2.2\,mm \times 1\,mm$) with a pitch of $3\,\mu m$ was encompassing the interface and is used for local strain measurements. An additional "macro grid" ($3\,mm \times 3\,mm$) with a pitch of $15\,\mu m$ was used for quick strain control during the experiment. Images were obtained after elastic unloading at the targeted strains and permitted to compute high resolution strain full-fields using the *Correlation Manual Value* (CMV) DIC software [5]. Moreover, HR-DIC data was overlapped on a distorsion corrected EBSD map [6] to associate strain localisation patterns with the microstructure.

3. Result and discussion

3.1. Microstructure

The microstructure of the RS is illustrated by polar figures of EBSD maps in Figure 1. Elongated grains along the building direction can be observed for the cross section, i.e. the normal plan, and the printing plan. The magnifying box of the cross section exhibits epitaxial growth of several grains at

the interface which insures a solid metallurgical bond [8]. Next, a quantitative analysis and the HR-DIC will be performed on the printing plan.
The grains are described by: (i) the equivalent grain diameter ϕ defined as the diameter of a disk with a surface equal to the grain area and (ii) the aspect ratio (AR) which corresponds to the ratio of the principal axes of the smallest circumscribed ellipse. The distribution of the microstructure characteristics (ϕ and AR) are expressed next by the mean values and their respective standard deviations.
We remark that substrate grains ($\phi = 7.2\,\mu m \pm 3.9\,\mu m$, AR$= 1.8 \pm 0.8$) are smaller and more equiaxed than grains in the repaired part ($\phi = 25.2\,\mu m \pm 21.2\,\mu m$, AR $= 2.4 \pm 1.3$).
The printed part features a complex microstructure. *Small* grains ($\phi < 15\,\mu m$) are scattered in the first layers and at several locations at the interlayers. The statistical data for *small* (more equiaxed) and *large* (columnar) grains are different, see table 1.

A herringbone pattern can be noticed in the printed part as discussed in [2; 7; 4]. It is a consequence of the shape of the melt pool solidification front and the back and forth printing strategy. The evolution of the equivalent grain diameter against distance from the interface is plotted in Figure 2(a), where the black stars correspond to the average ϕ per interface distance bin. One can notice that the grain size: (i) in substrate $[-1200\,\mu m\ ;\ 0\,\mu m]$ is small and constant, (ii) in the first deposited layers $[0\,\mu m\ ;\ 400\,\mu m]$ has a steep growth regime, (1) and (iii) in the printed material $[400\,\mu m\ ;\ 3800\,\mu m]$ has a moderate growth (2). The growth pattern is a consequence of the heat exchange in the wall. Heat accumulation increases with distance from the substrate and results in larger grains as reported in [3].

3.2. Mechanical properties

Tensile curves under monotonic loading for the FPS, RS and SS are displayed in Figure 2(b). As expected, the RS exhibits a mean tensile behavior with a lower ductility as already observed in [9; 10]. The RS fractured within the printed part, several millimeters from the interface, which indicates that the bonding zone is a strong link.

In Figure 3(a), (b) and (c) are displayed the distribution of the axial local strain component, i.e. ε_{11}, superimposed on the EBSD map for three global deformation steps corresponding to: $\simeq 2\,\%$, $\simeq 10\,\%$ and $\simeq 17\,\%$ respectively (see Figure 2(b)). Additionally, a complementary plot of the distribution of the mean value of ε_{11} along the direction 2 is equally proposed for the three

steps.

At $\varepsilon_{11} \simeq 2\,\%$, only the substrate is deformed as it presents the lowest yield strength, see Figure 2(b). The strain gradient follows an almost smooth increase from the interface into the inner substrate, a pattern that is equally found at higher global strains, see Figure 3(b) and (c). With increasing global strain, $\varepsilon_{11} \simeq 10\,\%$ or $\simeq 17\,\%$, the local strain increases in the printed part and is characterized by an important scatter correlating spatially with the position of the interlayers. Eventually, interlayers become regions with the highest local strain as displayed in Figure 3(c). For a similar loading on printed specimens, [4] equally observed localisation at interlayers and [11] reported that interlayers are a crack initiation area.

In the vicinity of the interface, an $\approx 200\,\mu m$ low deformation zone was observed. Microhardness measurements along the building direction exhibited a hardness increase in this area, highlighted in pink in Figure 3(d). This is a consequence of the heat affected zone in the substrate with strengthening effect [12]. In the printed part, this is justified by the finer microstructure of the first deposited layers as depicted by the regime (1) in Figure 2(a). As discussed in [13], finer strengthening mechanisms such as the evolution of the dislocation density and the compositional microsegregation with respect to the distance with the substrate are a further argument for the hardness increase.

4. Conclusion

The microstructural gradient of properties and the associated deformation mechanisms at the repair interface were studied for a 316L stainless steel hot rolled sheet substrate repaired by DED. We observed an indisputable difference of the microstructures: small equiaxed grains for the substrate and larger and elongated grains for the printed part. Additionally, during in situ tensile test in an SEM combined with HR-DIC and EBSD maps, the observed strain was homogeneous in the substrate part while exhibiting a heterogeneous pattern in the printed part with strain localisation at interlayers. An $\approx 200\,\mu m$ low deformation zone was observed at both sides of the interface and was associated with higher hardness.

Declaration of Competing Interest

None.

Acknowledgement

The authors would like to thank the *Direction Générale de l'Armement* (DGA), for the funding of the experimental printing facility and to acknowledge the help of Simon Allais for the SEM measurements and test.

Conflict of interest

None.

Figures:

	Printed part			Substrate part
	All grains	*small* grains	*large* grains	All grains
Average ϕ (μm)	25.2 ± 21.2	8.5 ± 3.5	36 ± 20.9	7.2 ± 3.9
Median ϕ (μm)	19.3	8.4	29.5	6.2
Average AR	2.4 ± 1.3	2.3 ± 1.3	2.7 ± 1.6	$1,8 \pm 0.6$
Median AR	2	2	2.2	1.6
Number of grains	8807	3463	5344	42014
Surface occupied (%)	100	13.3	86.7	100
Surface of study (mm^2)	3.8×2			

Table 1: Mean value of the microstructure characteristics (ϕ and AR) and their respective standard deviations. Additional microstructure statistics are equally specified.

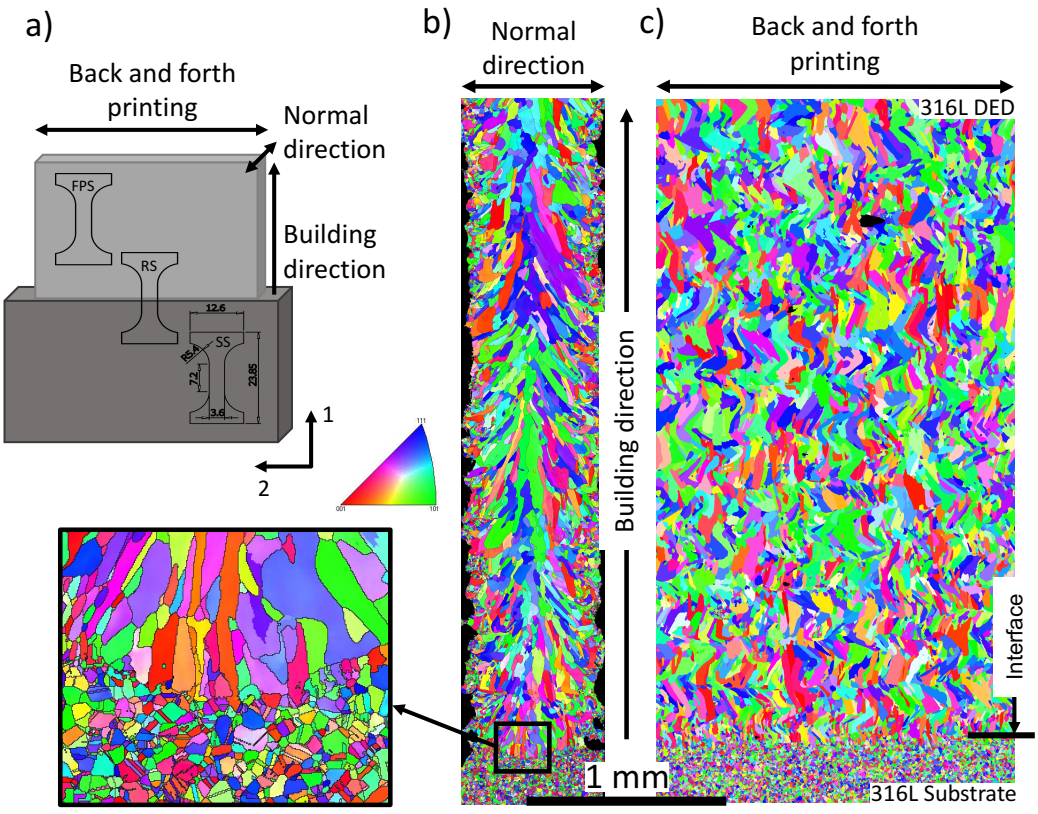

Figure 1: (a): Design scheme of the fully printed specimen, repaired specimen and substrate specimen denoted as FPS, RS and SS respectively. The dimensions of the geometry displayed for the SS are common for the three configuration.
EBSD maps of the repaired specimen for the normal and printing plans in (b) and (c) respectively.

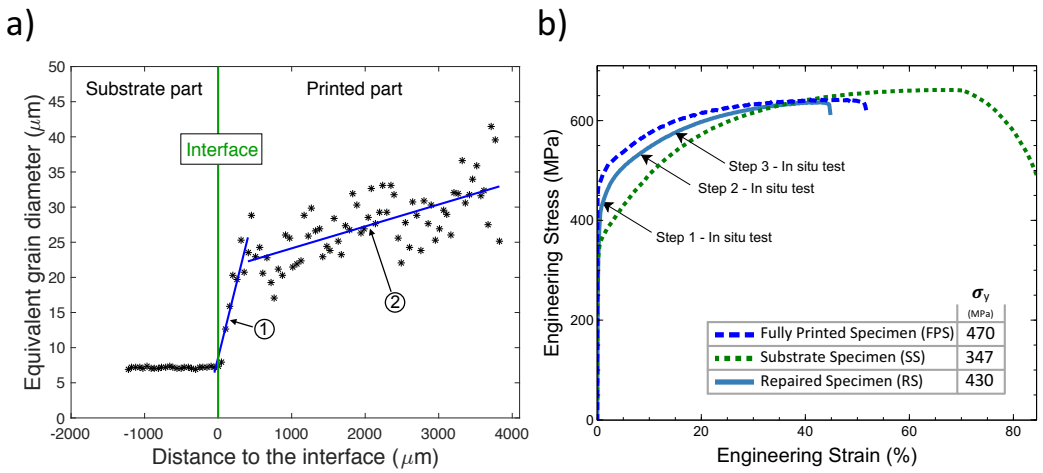

Figure 2: (a): Evolution of the equivalent grain diameter (ϕ) with respect to its distance from the interface for the repaired specimen. The grains were gathers into bins with respect to the distance to the interface of their respective center of gravity. 2 regimes of the evolution of ϕ can be observed in the printed par highlighted by linear squares fitting curves (1) ($\phi = 0.04x + 8.6$) and (2)($\phi = 0.003x + 21$) (b): Tensile engineering stress-strain curves and their respective yield strengths (σ_y)

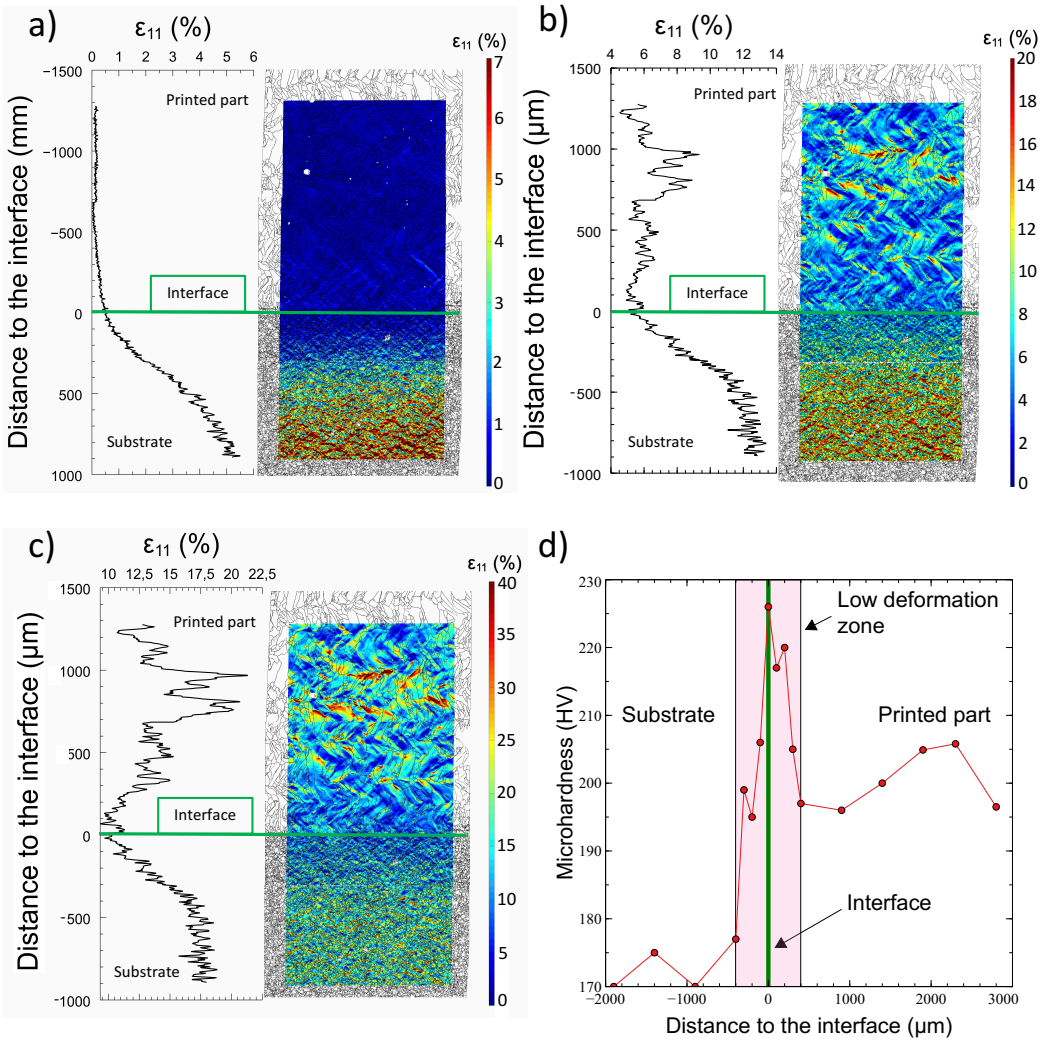

Figure 3: Evolution of the axial strain for the step of deformation 1, 2 and 3 (see Figure 2(b)) respectively in (a) (b) and (c). The deformation ϵ_{11} obtained by DIC is overlapped on the microstructure obtained by EBSD and a complementary plot of the evolution of the mean ϵ_{11} with respect to the distance to the interface is proposed. (d): Microhardness map showing higher hardness around the interface of the repaired zone corresponding to the low deformation zone.

[1] B. Onuike, A. Bandyopadhyay, Mater. Lett. 252 (2019) 256259.

[2] L.L. Parimi, G. Ravi, D. Clark, M.M. Attallah, Mater. Charact. 89 (2014) 102111.

[3] Z. Wang, T.A. Palmer, A.M. Beese, Acta Mater. 110 (2016) 226235.

[4] Y. Balit, E. Charkaluk, A. Constantinescu, Addit. Manuf. 31 (2020) 100862.

[5] L. Allais, M. Bornert, T. Bretheau, D. Caldemaison, Acta Metall. Mater. 42 (1994) 38653880.

[6] Y.B. Zhang, A. Elbrond, F.X. Lin, Mater. Charact. 96 (2014) 158165.

[7] G.P. Dinda, A.K. Dasgupta, J. Mazumder, Surf. Coatings Technol. 206 (2012) 21522160.

[8] V. Ocelìk, I. Furár, J.T.M. De Hosson, Acta Mater. 58 (2010) 67636772.

[9] Y. Zhu, J. Li, X. Tian, H. Wang, D. Liu, Mater. Sci. Eng. A 607 (2014) 427434.

[10] Z. Zhao, J. Chen, H. Tan, X. Lin, W. Huang, Opt. Laser Technol. 92 (2017) 3643.

[11] K. Zhang, S. Wang, W. Liu, X. Shang, Mater. Des. 55 (2014) 104119.

[12] W.J. Oh, W.J. Lee, M.S. Kim, J.B. Jeon, D.S. Shim, Opt. Laser Technol. 117 (2019) 617.

[13] T.R. Smith, J.D. Joshua, C. San Marchi, J.M. Schoenung, Acta. Mater. 164 (2019) 728-740.